# Directed by Directionality: Benefiting from the Gain Pattern of Active RFID Badges

Yang Zhao, *Student Member*, *IEEE*, Neal Patwari, *Member*, *IEEE*,
Piyush Agrawal, *Student Member*, *IEEE*, and Michael G. Rabbat, *Member*, *IEEE*

**Abstract**—Tracking of people via active badges is important for location-aware computing and for security applications. However, the human body has a major effect on the antenna gain pattern of the device that the person is wearing. In this paper, the gain pattern due to the effect of the human body is experimentally measured and represented by a first-order directional gain pattern model. A method is presented to estimate the model parameters from multiple received signal strength (RSS) measurements. An alternating gain and position estimation (AGAPE) algorithm is proposed to jointly estimate the orientation and the position of the badge using RSS measurements at known-position anchor nodes. Lower bounds on mean squared error (MSE) and experimental results are presented that both show that the accuracy of position estimates can be greatly improved by including orientation estimates in the localization system. Next, we propose a new tracking filter that accepts orientation estimates as input, which we call the orientation-enhanced extended Kalman filter (OE-EKF), which improves tracking accuracy in active RFID tracking systems.

**Index Terms**—Wireless sensor networks, radio propagation, localization, tracking.

## 1 Introduction

Received signal strength (RSS)-based radio localization and tracking of people and assets has significant benefits for logistics, security, and safety [1], [2]. Most RSS-based methods make the assumption that transmitter badges attached to objects or carried by people have isotropic gain patterns. However, even when a transmitter badge has an antenna that is considered isotropic, the person or object has considerable effect on the badge's radiation by: absorbing power, altering the antenna impedance and thus its radiation efficiency, and distorting the antenna gain pattern [3], [4]. In this paper, we develop models and methods to handle, and in fact benefit from, the removal of the unrealistic isotropic gain pattern assumption.

Real-world directional gain patterns are problematic for both fingerprint-based and model-based RSS localization algorithms. In fingerprint-based localization, exhaustive calibration measurements are performed in the environment of interest, in which a person carries a transmitter to each location, and perhaps each facing direction, while its RSS is measured [1], [5]. The gain pattern that existed during the calibration period is assumed to hold for all transmitter badges, regardless of to what object or person they are attached. In model-based algorithms, a model relating RSS and path length is assumed [6] or estimated from training measurements [7]. When the gain pattern is no longer isotropic, in some directions, the RSS will increase, while in some other directions, the RSS will decrease. Based on the data, model-based algorithms will infer that the transmitter is closer to receivers which measured larger RSS and will thus produce estimates which are biased toward directions of high gain in the gain pattern. In this paper, we focus on improving the robustness of model-based algorithms to real-world directional gain patterns.

In localization experiments, we find that position estimates are often biased because of a nonisotropic gain pattern. An example is shown in Fig. 1. In an experiment described in Section 3.5.1, a person wears a transmitter badge on his chest, and is located using the model-based maximum likelihood estimation (MLE) algorithm that assumes isotropic gain pattern [6], which we call the naive MLE algorithm. When the person wearing the badge is facing North, the badge position estimate is biased to the North of its actual position; if the person is headed East, the badge position estimate is biased to the East of its actual position, etc. Essentially, the naive MLE estimates that the badge is closer to receivers that measure more power, and receivers in the direction the person is facing receive more power than would be predicted by an isotropic model.

Previous studies have focused on characterizing the effects of a human body's location and orientation on RSS measurements [1], [8], [9], [10], [11]. However, we are unaware of research progress in the effort to include gain pattern in model-based RSS localization algorithms. We demonstrate progress in this direction.

To develop an improved model-based algorithm, we first require a model for the directionality of a transmitter badge when worn by a person or attached to an object. We focus on the problem of a transmitter badge worn by a person. However, we believe that tags attached to large objects will generally experience nonisotropic gain patterns as well, so

- *Y. Zhao, N. Patwari, and P. Agrawal are with the Department of Electrical and Computer Engineering, University of Utah, 50 S. Central Campus Drive, MEB Room 3280, Salt Lake City, UT 84112. E-mail: yang.zhao@utah.edu, {npatwari, pagrawal}@ece.utah.edu.*
- *M.G. Rabbat is with the Department of Electrical and Computer Engineering, McGill University, McConnell Engineering, Room 639, 3480 University Street, Montréal, QC H3A 2A7, Canada. E-mail: michael.rabbat@mcgill.ca.*

*Manuscript received 14 July 2010; revised 16 Mar. 2011; accepted 18 Mar. 2011; published online 27 Apr. 2011.*
*For information on obtaining reprints of this article, please send e-mail to: tmc@computer.org, and reference IEEECS Log Number TMC-2010-07-0339. Digital Object Identifier no. 10.1109/TMC.2011.89.*

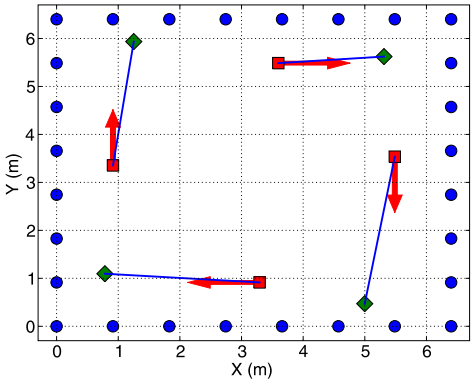


Fig. 1. Position estimate error due to nonisotropic gain pattern (anchor node positions (•); actual badge positions (■); MLE estimates (◆); walking directions (⇒)).

extensions to other types of tagged objects are feasible. We perform experiments to measure the variation of RSS as a function of the person's orientation (i.e., facing direction). Based on the results, we propose a first-order model to capture most of the variation in the gain pattern as a function of user orientation. We also present a method to estimate user orientation and directionality from ordinary RSS measurements collected by the network.

Next, we include the gain pattern model in the RSS-distance model to jointly estimate the position and orientation of people in RF sensor networks. An alternating gain and position estimation (AGAPE) algorithm is developed to jointly estimate the position, orientation, and gain pattern of the badge. Experimental results show that the root mean squared error (RMSE) can be greatly reduced by including the orientation estimate in the localization. For example, in one experiment, the RMSE from the naive MLE algorithm is 2.65 meters, while the RMSE from the proposed algorithm is 0.87 meters, a 67 percent reduction.

It is not obvious that a nonisotropic gain pattern can benefit coordinate localization, because of the required additional "nuisance" parameters which must be estimated. We provide theoretical results that show that having a gain pattern is not an impediment for localization algorithms—*the existence of a directional gain pattern can actually reduce position error*. For this result, we derive the Bayesian Cramér-Rao bound (Bayesian CRB) for joint estimation of orientation and position. The Bayesian CRB provides the lower bound on the mean squared error (MSE) of any estimator [12]. Comparison between the Bayesian CRB and CRB derived with an isotropic gain pattern assumption [6] shows that joint estimation of orientation and position may outperform (result in lower MSE) estimation of position alone in the isotropic case.

We also present results that show that tracking is improved by joint position and orientation estimation. Regardless of whether one uses the gain pattern in a localization algorithm or not, it is often important to track a badge's position over time to reduce uncertainty in an object or person's path. When a person wears a transmitter badge in a consistent location on their body, we can infer from their orientation which direction they will be moving, since people tend to walk forward (much more than backwards or sideways). We include this intuition to develop a Kalman tracking method which uses orientation estimates as input, which we call the orientation-enhanced extended Kalman filter (OE-EKF). Traditional Kalman filters and extended Kalman filters use only coordinate estimates as input, even though they are used to estimate velocity (and thus direction). Our OE-EKF is distinct because it uses estimated orientation *as an input*, in addition to providing estimated velocity. We find knowing orientation can also help improve the accuracy of tracking.

In summary, the contribution of this paper is to show that real-world nonisotropic gain patterns of transmitter badges are not a problem to be ignored, but a means to improved localization and tracking performance. We propose a first-order gain pattern model and validate it from a set of measurements. We develop an algorithm to estimate gain pattern from RSS measurements, and an alternating gain and position estimation algorithm. The Bayesian CRB for the joint estimation problem is derived and compared to that for position estimation with isotropic gain patterns. Finally, an orientation-enhanced extended Kalman filter is implemented to track mobile users in RF sensor networks.

The rest of this paper is organized as follows: Section 2 proposes a method to estimate the gain pattern of a transmitter badge. Section 3 investigates joint position and orientation estimation, including experimental and theoretical results. Section 4 investigates tracking, using standard Kalman filters and a new OE-EKF method. Related work is presented in Section 5, and finally we conclude in Section 6.

## 2 Models

Any improvement of model-based RSS localization algorithms must begin with statistical models that are based on real-world measurements. In this section, we present measurement-based models for the gain pattern of a transmitter badge worn by a person. A transmitter in close proximity to a human body is strongly affected by that proximity. Human tissue absorbs power sent in its direction and distorts the gain pattern of the transmitter [3], [4].

A general model for the dBm power $P_i$ received at anchor node $i$ from transmitter badge $t$, is the log-distance model [13]. Including the transmitter gain pattern, the dBm power $P_i$ is modeled as

$$P_i = P_0 - 10n_p \log_{10}\left(\frac{d_i}{d_0}\right) + g(\alpha_i) + \eta, \qquad (1)$$

where $P_0$ is the received power in dBm at a reference distance $d_0$, $n_p$ is the pathloss exponent, $d_i = \|\mathbf{z}_i - \mathbf{z}_t\|$ is the distance between anchor node $i$ at coordinate $\mathbf{z}_i$ and transmitter badge $t$ at coordinate $\mathbf{z}_t$, $\alpha_i$ is the angle between anchor node $i$ and the badge, $g(\alpha_i)$ is the gain pattern in dB of the transmitter badge at angle $\alpha_i$, and $\eta$ is the model error plus noise. In practice, we estimate $n_p$ and $P_0$ using the received power measurements between pairs of anchor nodes. Assuming known anchor node coordinates, we estimate $n_p$ and $P_0$ via linear regression, as in [6].

Naive model-based localization algorithms use $g(\alpha_i) = 0$ for all $\alpha_i$. We propose to include a nonzero $g(\alpha_i)$ in (1). Note that the function must be periodic since $g(\alpha_i) = g(\alpha_i + 2\pi)$ for any $\alpha_i$. Any real-world gain pattern will depend on the

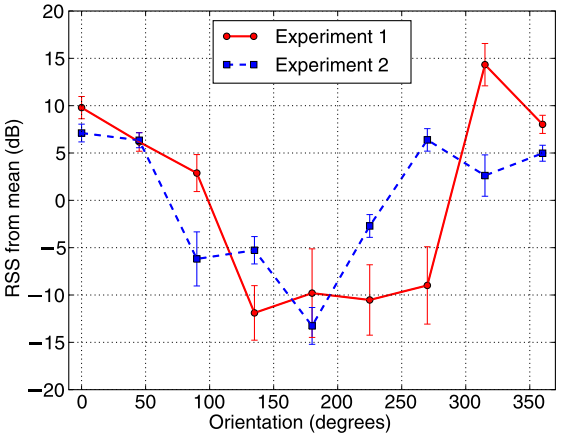


(a)

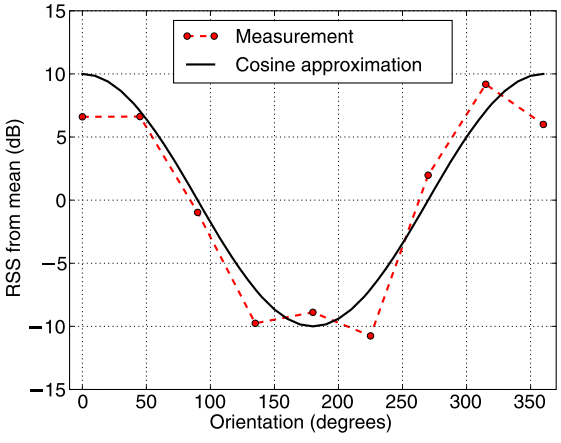


(b)

Fig. 2. Human body effect on gain pattern (RSS from mean). (a) Measured gain patterns and $1-\sigma$ error bars in two different experiments (Gain pattern at each orientation is averaged over about 400 measurements during a period of 20 seconds); (b) Average over all measured data (Gain pattern is maximum when person is facing 0 degrees to the other sensor).

person and the badge, and will look somewhat random; however, we hope to capture the major features of $g(\alpha_i)$ that will be largely accurate for the average person.

Section 2.1 presents a measurement campaign to characterize average behavior of gain patterns. Based on these measurements, we formulate a model in Section 2.2 and evaluate the model in Section 2.3.

### 2.1 Measurements

We perform several experiments to quantify the effect of the orientation (facing direction) of a human body on the RSS measured from the transmitter that the person is wearing. We use two Crossbow TelosB nodes operating at 2.4 GHz. One node (node 1) is placed on a stand, and the other one (node 2) is worn by a person, hanging in the middle of his chest. While keeping the distance between these two nodes the same, the person wearing node 2 turns 45 degrees every 20 seconds. Node 2 transmits about 20 times per second, and the RSS at node 1 is recorded on a laptop. Thus, about 400 RSS measurements are recorded for each of the eight different orientations. The above experiment is repeated eight times by five different people wearing the badge in the student recreation building and an empty parking lot at the University of Utah. The distances between the two nodes

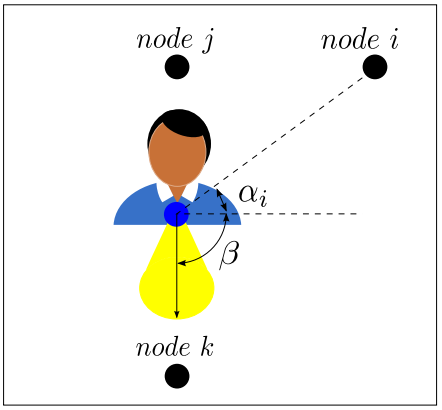


Fig. 3. Gain pattern of a badge in a network.

are varied from 1.5 to 5.0 meters in these eight different experiments. A total of 25,600 measurements are recorded.

As expected, individual measured gain patterns are unique. Fig. 2a shows the measurements from two different experiments. In both experiments, the minimum RSS are at either 180 or 145 degrees, and the maximum RSS are at 0 or 315 degrees. The mean gain pattern, averaged across all experiments, is shown in Fig. 2b. We see that if the person's orientation is 180 degrees, i.e., the human body blocks the line-of-sight (LOS) path between node 1 and node 2, the gain pattern is close to the minimum. If the person is facing node 1, i.e., an orientation of 0 degrees, then the gain pattern is about 20 dB higher than at its lowest point. The average gain pattern closely resembles a cosine function with period 360 degrees and an amplitude 10 dB.

We note that the variation we see in received power as a function of angle due to the presence of the human is similar to results from other measurement studies [5], [10].

### 2.2 Gain Pattern Model

Based on the results of the measurements, we propose a model for the gain pattern $\hat{g}(\alpha)$, as a cosine function with period 360 degrees

$$\hat{g}(\alpha) = G_1 \cos(\alpha - \beta), \tag{2}$$

where $\beta$ is the orientation (direction of maximum gain) of the badge (see Fig. 3), and $G_1 \geq 0$ is the magnitude of the cosine function in dB. We also refer to $G_1$ as the directionality, because high $G_1$ indicates that badge's pattern is highly directive in one direction, while $G_1 = 0$ indicates no directionality, i.e., the badge is an isotropic radiator.[1]

There are two main reasons to use the model of (2). First, the model represents the two most important characteristics observed in the measurements, regardless of path length or person wearing the badge: that the gain is higher in the direction the person is facing, and lower in the direction opposite. In an RF sensor network with several anchor nodes, suppose a user wearing a badge stands halfway between node $j$ and node $k$ facing node $k$, as shown in Fig. 3. Then, based on our measurements, the mean RSS value of node $k$

1. The standard definition of directivity is related to the maximum gain across both elevation and azimuth angles; here we consider only azimuth angles, effectively assuming the maximum directive gain is along the azimuth [14].

would be greater than that of node $j$, although the distances between the badge and these two nodes are the same.

The second reason to use (2) is that it is a first-order model for any periodic function, and for this data in particular, the measurements show a single order captures the vast majority of the angular variation. Any function with period $2\pi$ has a Fourier series representation as a sum of sines and cosines at frequencies that are integer multiples of $\frac{1}{2\pi}$:

$$g(\alpha) = \frac{1}{2\pi} \sum_{k=-\infty}^{\infty} G(k) e^{j2\pi k\alpha},$$

where $G(k)$ are the complex-valued Fourier series components [15]. When $g(\alpha)$ is purely real, then $G(-1)$ and $G(1)$ are complex conjugates, and thus $G(-1) + G(1) = 2\mathbb{R}\{G(1)\}$, where $\mathbb{R}$ is the real operator. As a result

$$g(\alpha) = \frac{1}{2\pi} G(0) + \frac{1}{\pi} \mathbb{R}\left\{ \sum_{k=1}^{\infty} G(k) e^{j2\pi k\alpha} \right\}. \tag{3}$$

The model of (2) is simply the first harmonic of an arbitrary gain pattern measurement. That is, we include only the $k = 1$ term in (3).

### 2.3 Gain Pattern Model Evaluation

When measuring the gain pattern at discrete values of $\alpha_i, i = 0, 1, \ldots N-1$, we require the discrete Fourier transform (DFT) instead of the Fourier series. However, the same principle applies—the cosine with period $2\pi$ is the first-order approximation of the gain function. Specifically, for the gain pattern at angle $\alpha_i$, the discrete-time exponential representation is given by

$$\begin{aligned} g(\alpha_i) &= \frac{1}{N} \sum_{k=0}^{N-1} G(k) e^{j\alpha_i k} \\ &= \frac{1}{N} G(0) + \frac{2}{N} \mathbb{R}\left\{ \sum_{k=1}^{M} G(k) e^{j\alpha_i k} \right\} \\ &= \frac{1}{N} G(0) + \frac{2}{N} \sum_{k=1}^{M} |G(k)| \cos(\angle G(k) + \alpha_i k), \end{aligned} \tag{4}$$

where $M = \frac{N}{2}$, and $\alpha_i = \frac{2\pi i}{N}$, for $N$ equally spaced measurements. In the measurement experiments, we had $N = 8$.

The mean gain $G(0)$ is simply the average of all of the differences (which we call the model error) between $P_i$ and the log-distance path loss model, that is, $P_0 - 10n_p \log_{10}(d_i/d_0)$. Because $n_p$ and $P_0$ are determined by linear regression, they tend to make the model error zero mean. Thus, we assume that $G(0) = 0$ dB because any mean model error would have been removed by the linear regression. Then, the gain pattern from an $M$ order model can be estimated as

$$\hat{g}_M(\alpha_i) = \frac{2}{N} \sum_{k=1}^{M} |G(k)| \cos(\angle G(k) + \alpha_i k). \tag{5}$$

The first-order model including only the $k = 1$ term in (5), is

$$\hat{g}(\alpha_i) = \frac{2}{N} |G(1)| \cos(\angle G(1) + \alpha_i). \tag{6}$$

To evaluate the first-order model for the gain pattern at discrete values, we use it to recover the mean gain pattern (shown in Fig. 2b) obtained from eight experiments of the measurement campaign. We also use the zero-order model, i.e., with only DC component $G(0)$ in (4), and the second, third, fourth order models to recover the actual gain pattern. The relative approximation errors are shown in Fig. 4. We see that if we only use the DC component $G(0)$, the relative approximation error is 100 percent. If we use the first-order model, the relative error decreases dramatically to less than 30 percent. If we use higher order models, the relative error continues to decrease, but only decreases slightly as more DFT terms $G(k)$ are added. We note that, using a zero-order model with $G(0) = 0$ is equivalent to using an isotropic gain pattern assumption. Fig. 4 shows that the approximation error from the first-order model is about 70 percent less than that from the zero-order model. So the first-order model is much more accurate than the zero-order model with isotropic gain pattern assumption. Although using higher order models can further reduce the approximation error, the reduction of error is not so significant compared to the reduction from the zero-order model to the first-order model. Using higher order models also requires more parameters, which increases the problem of overfitting. Thus, we propose to use the first-order sinusoidal model to quantify the effect of the human body orientation on RSS measurements.

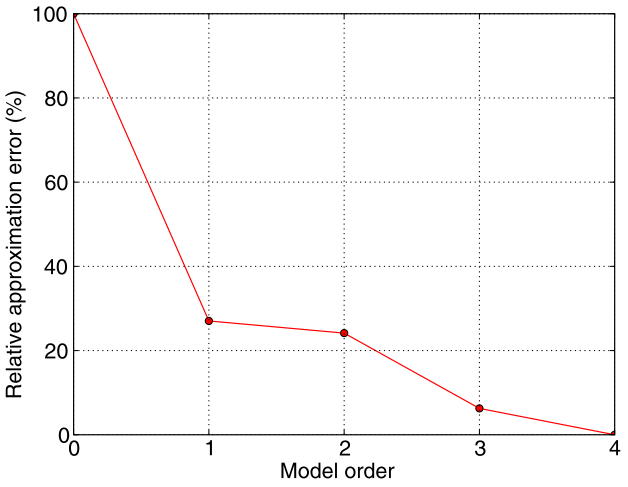


Fig. 4. Relative approximation error versus model order (number 0 corresponds to the isotropic gain model, number 1 corresponds to the first-order model; the approximation error is relative to the error of the isotropic gain model).

## 3 Localization Using Orientation

### 3.1 Problem Statement

In this section, we focus on 2D position estimation using RSS measurements. For a network with $N$ anchor nodes and one badge (we use one badge to simplify notation, but extension to multiple badges is possible), the position estimation problem corresponds to the estimation of the coordinates of the badge $\mathbf{z}_t = [x_t, y_t]^T$. However, from (2), two parameters in the gain pattern model must be estimated. So we include these two parameters as nuisance parameters, and the unknown parameter vector $\boldsymbol{\theta}$ becomes

$$\boldsymbol{\theta} = \left[\mathbf{z}_t^T, \beta, G_1\right]^T, \tag{7}$$

where $\beta$ is the orientation of the badge, and $G_1$ is the directionality of the gain pattern.

### 3.2 Baseline Algorithm

To estimate both the badge position and the gain pattern, a baseline algorithm—4D maximum likelihood estimation algorithm is introduced here for algorithm comparison and analysis.

As discussed in Section 2, the received dBm power $P_i$ is modeled as (1). Assuming the RSS values $P_i$ are independent Gaussian with variance $\sigma^2$, and mean $\mu(\boldsymbol{\theta}) = P_0 - 10n_p \log_{10}(d_i/d_0) + g(\alpha_i)$, one can show that the MLE of the badge position is

$$\hat{\boldsymbol{\theta}}_{MLE} = \arg\max_{\theta} \sum_{i=0}^{N-1} (P_i - \mu(\boldsymbol{\theta}))^2. \tag{8}$$

One way to find the MLE solution is to use the grid search method. For example, the TI CC2431 uses a 2D grid search method to find the MLE coordinate estimate for the isotropic gain pattern case [16]. However, as the dimension of the estimation parameter vector $\boldsymbol{\theta}$ increases, the computation time of grid search increases exponentially. Since we have four parameters in $\boldsymbol{\theta}$, a 4D grid search method can be used to obtain the MLE solution for analysis, but the high computation cost prohibits it from real-time applications. To jointly estimate the position and the gain pattern, a different algorithm must be used.

### 3.3 Gain Pattern Estimator

Before we propose the algorithm to jointly estimate the position and the gain pattern, we first introduce a gain pattern estimator, assuming we know the badge position $\mathbf{z}_t$.

By comparing (6) and (2) in Section 2, we find the two model parameters $\beta$ and $G_1$ of the gain pattern can be calculated as

$$\begin{aligned} \beta &= -\angle G(1), \\ G_1 &= \frac{2}{N}|G(1)|. \end{aligned} \tag{9}$$

Thus, to estimate the gain pattern, the DFT term $G(1)$ needs to be calculated first.

In the measurement experiments discussed in Section 2.1, it was possible to measure the gain at equally spaced angles. In real deployments, anchor nodes will make measurements at a variety of nonequally spaced angles $\alpha_i$, depending on badge and anchor node positions. The most common way to estimate the spectral content in a signal using nonequally spaced samples is simply to apply the DFT to the available samples [17]. Thus, we estimate $G(k)$ as

$$G(k) = \sum_{i=0}^{N-1} g(\alpha_i) e^{-j\alpha_i k}. \tag{10}$$

To calculate $g(\alpha_i)$ in (10), rewriting (1), we have

$$g(\alpha_i) = P_i - P_0 + 10n_p \log_{10} \frac{d_i}{d_0}, \tag{11}$$

where $\alpha_i$ is the angle between anchor node $i$ and badge

$$\alpha_i = \operatorname{atan}\left(\frac{y_i - y_t}{x_i - x_t}\right).$$

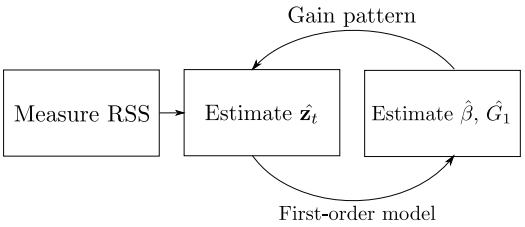


Fig. 5. Flowchart of the AGAPE algorithm.

Note we need only $G(1)$ for the first-order model of (2). This calculation of $G(1)$ requires only $N$ complex multiplies and adds, where $N$ is the number of RSS measurements received for a badge. This low complexity is important to minimize the computational complexity of the localization algorithm.

### 3.4 Alternating Gain and Position Estimator

In the gain pattern estimator, we assumed known badge position, which in general, is unknown. For joint position and gain pattern estimation, in this section, we propose an alternating gain and position estimation algorithm to efficiently estimate both the position and orientation of the user wearing a badge in an RF sensor network.

The basic idea of this algorithm is to first estimate the position of the badge, and take advantage of the first-order sinusoidal model to calculate the gain pattern parameters. Given the gain pattern, we use the RSS-distance model (1) to reestimate the position of the badge. The algorithm iterates until a misfit function is minimized. We note that the proposed AGAPE algorithm is a form of alternating minimization method [18].

The flowchart of the AGAPE algorithm is shown in Fig. 5, and the detailed procedure is discussed here. For the first step, assuming the gain pattern is isotropic, we use the naive MLE method to estimate the badge position based on the RSS-distance model in [6]. The MLE solution can be found via a conjugate gradient algorithm [6], here, we use a 2D grid search method in the position estimation step to avoid the local minima problem from a numerical method. Again, we note that 2D MLE grid search can be accomplished quickly in hardware [16]. The output of the position estimation step, we refer to as $\hat{\mathbf{z}}_t$.

The next step is the orientation estimation step. Given an estimated position, we calculate the gain pattern $g(\alpha_i)$ from the RSS-distance model (1)

$$g(\alpha_i) = P_i - P_0 + 10n_p \log_{10} \frac{\|\hat{\mathbf{z}}_t - \mathbf{z}_i\|}{d_0}. \tag{12}$$

And then, $G(1)$ is calculated from (10). After that, the orientation $\beta$ is estimated from the phase angle of $G(1)$, and the directionality $G_1$ is estimated from the magnitude of $G(1)$, as given in (9). Finally, we use the estimated $\hat{\beta}$ and $\hat{G}_1$ in the RSS-distance model to estimate the position of the badge $\hat{\mathbf{z}}_t$ again.

The steps of position estimation and orientation estimation repeat until the following misfit function is minimized

$$\Phi = \sum_{i=1}^{N} \left(P_i - \hat{P}_i\right)^2, \tag{13}$$

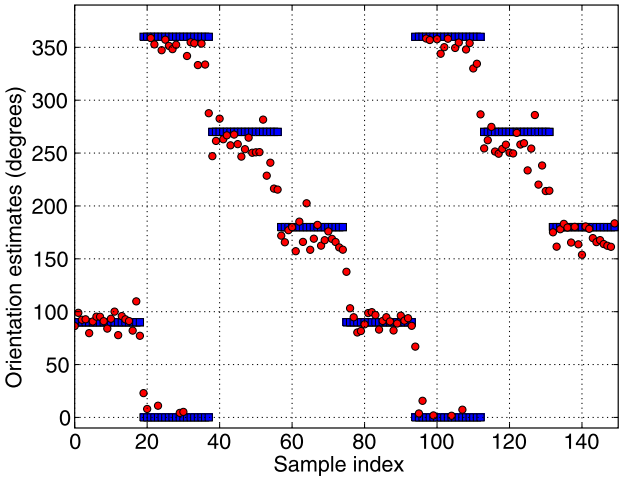


Fig. 6. Mobile's actual orientations (■) and orientation estimates (•) (time for each sample is about 0.4 seconds).

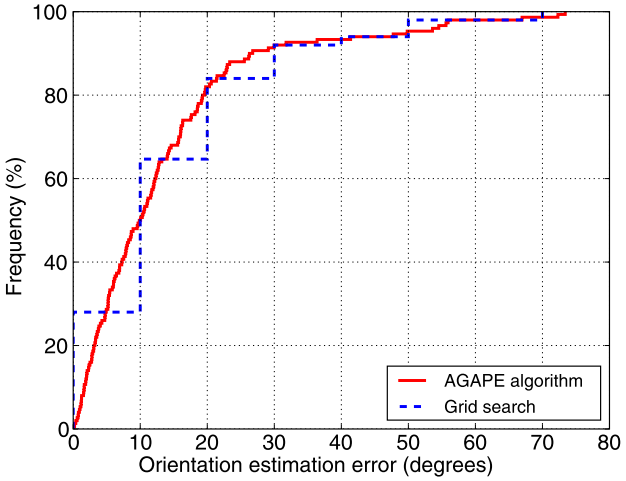


Fig. 7. CDF of orientation estimation error.

where $\hat{P}_i$ is the RSS estimate at anchor node $i$, which is calculated from the RSS-distance model (1) using estimated badge position $\hat{\mathbf{z}}_t$, and estimated gain parameters $\hat{\beta}$ and $\hat{G}_1$. We do not study convergence results for the AGAPE algorithm. Since minimizing (13) corresponds to a nonlinear least squares problem, we expect that AGAPE will be trapped in local minima. To avoid reporting local minima, we rerun the algorithm from different initial conditions. We fix the initial values of $G_1$ to a nonzero value, set the initial values of $\beta$ to a combination of four different orientations, i.e., 0, 90, 180, and 270 degrees, perform AGAPE for each initial condition and choose the result with the minimum misfit function as the final result.

## 3.5 Experiment and Results

### 3.5.1 Experiment Description

Three localization experiments are performed in a 6.4 m by 6.4 m area outside the Merrill Engineering Building of the University of Utah. This grassy area is near trees and 3 m away from the building wall. The area is surrounded by 28 TelosB anchor nodes deployed at known locations on stands at 1 m height. The nodes are programmed with TinyOS program Spin [19] to allow collection and recording of pairwise RSS measurements.

First, we measure pairwise RSS measurements between anchor nodes. Since the locations of the anchor nodes are known, we use the measured RSS and the link length to estimate the $n_p$ and $P_0$ parameters of the log-distance model of (1). Then, a person wears a TelosB node in the middle of his chest, and walks on a marked path at a constant speed of about 0.5 m/s. We ensure a constant speed using a metered path and a metronome. For example, in one experiment (Experiment 1), a person walks twice around a marked square path. Since the square path is marked and the person walks at a constant speed, the actual positions of the person are known at all times. Also, the person always walks forward in a straight line along each side of the square path, so the orientation of the badge is always identical to his walking direction. In the other two experiments (Experiments 2 and 3), another TelosB node is worn by another person. He walks on a marked rectangular path and a marked square path, respectively, in Experiments 2 and 3. The actual positions and orientations of the badge during these experiments are both known, so we can compare them with the position and orientation estimates from the AGAPE algorithm.

### 3.5.2 Experimental Results

For Experiment 1, the estimated orientations are shown in Fig. 6, together with the actual walking directions (badge orientations). The orientation estimates generally agree well with the actual orientations. The deviations from the actual orientations are generally less than 30 degrees. However, sometimes when the person is turning, the bias is larger than 30 degrees. This may be due to the fact that the algorithm uses RSS measurements from 28 anchor nodes to estimate the person's orientations, and at the turning points, RSS measurements may be a mix of those recorded before, after, and during turning.

The cumulative distribution function (CDF) of the orientation estimation error is shown in Fig. 7. The median error from the AGAPE algorithm is about 10 degrees, and more than 90 percent errors are below 30 degrees. Also shown in Fig. 7 is the CDF of orientation error from the MLE 4D grid search method. The MLE 4D grid search method searches every 10 degrees for the MLE solution of the orientation. While the grid search method takes much more time (on the order of 10 times more than the AGAPE algorithm in our Python implementation), the estimates are not more accurate than those from AGAPE. The median error from the grid search method is also 10 degrees.

Besides the orientation of the badge, another nuisance parameter $G_1$ is also estimated. The average value of the estimated $G_1$ is 12, which suggests that the directionality of the gain of the transmitter badge worn by this particular person in this particular environment is about 12 dB. This value is consistent with the results from our measurement campaign discussed in Section 2.1.

The most important result that we are interested in is the performance of position estimation. The CDF of the position estimation error is shown in Fig. 8. The median error of the position estimates is about 0.61 m, and about 90 percent of the estimation error is below 1.22 m. However, for the naive MLE method, the median error is 2.60 m, which is about 4.3

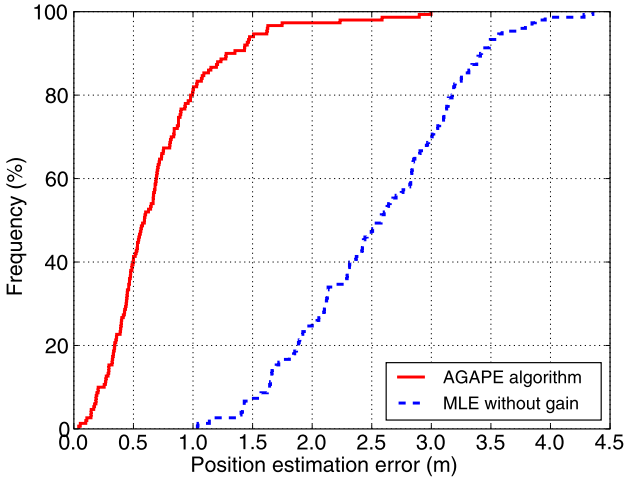


Fig. 8. CDF of position estimation error.

times larger than that from AGAPE. From the comparison of the CDFs, we see that significant improvement is made if we include the orientation estimate in the localization.

We also compare the root mean squared error of the position estimates, which is defined as

$$RMSE = \sqrt{\frac{1}{K}\sum_{k=0}^{K-1}\left(\hat{x}_t^{(k)} - x_0\right)^2 + \left(\hat{y}_t^{(k)} - y_0\right)^2}, \qquad (14)$$

where $\hat{x}_t^{(k)}$, $\hat{y}_t^{(k)}$ are estimated coordinates at time $k$, and $x_0$, $y_0$ are actual coordinates.

The RMSEs from the AGAPE algorithm of all three experiments are listed in Table 1. Also listed are the RMSEs from the naive MLE 2D method, and the RMSEs from the MLE 4D grid search method. We see that for Experiment 1, the RMSE from AGAPE is 0.87 m, which is similar to the MLE 4D grid search method. However, the MLE 4D grid search method, due to its computational complexity, is not a real-time algorithm. The RMSE from the naive MLE 2D method with an isotropic gain pattern assumption is 2.64 m. So for Experiment 1, the RMSE from AGAPE is reduced by 67.2 percent compared to the MLE 2D method. For Experiments 2 and 3, the RMSEs are reduced by 65.4 and 68.9 percent, respectively.

### 3.5.3 Effect of Number of Anchor Nodes

In the three experiments discussed above, we use 28 anchor nodes to locate a badge in a 6.4 m by 6.4 m square area. In some applications, we may not be able to have so many anchor nodes. To see the effect of node number on the localization accuracy of the AGAPE algorithm, we perform the following tests by using RSS measurements from only a fraction of all anchor nodes.

TABLE 1
Experimental Localization Results: RMSEs from MLE (2D), MLE (4D) and AGAPE

| RMSE (in meter) | MLE (2-D) | MLE (4-D) | AGAPE |
|---|---|---|---|
| Experiment 1 | 2.64 | 0.92 | 0.87 |
| Experiment 2 | 2.98 | 0.98 | 1.03 |
| Experiment 3 | 2.80 | 0.86 | 0.87 |

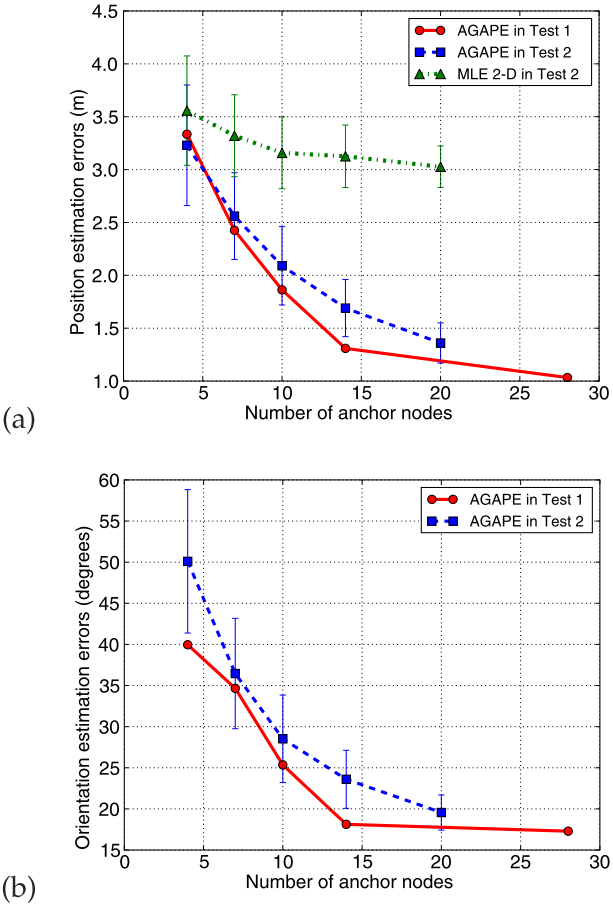


Fig. 9. Effect of node number on estimation error. (a) Position estimation error; (b) Orientation estimation error. (Test 1 uses equally spaced anchor nodes, and Test 2 uses randomly chosen anchor nodes).

In the first test—Test 1, we use RSS measurements from different numbers of equally spaced anchor nodes to locate the badge. For example, using the data collected in Experiment 2, we first choose the RSS measurements from four anchor nodes at each corner of the square area. As expected, the localization is not very accurate, the RMSE of the position estimate is 3.36 m, and the RMSE of the orientation estimate is 40 degrees. Next, we use the RSS measurements from those anchor nodes whose ID numbers are multiples of 1, 2, 3, and 4 (since the anchor nodes are placed in a numerically increasing order around the experimental area, these anchor nodes are equally spaced). The RMSEs of the position and orientation estimates are shown as dots (•) in Figs. 9a and 9b, respectively. We see that as the node number increases, the RMSEs of position and orientation estimates both decrease. When the node number increases to 14, the RMSE of the position estimate decreases to 1.30 m, and the RMSE of the orientation estimate decreases to 18 degrees. Further increase of anchor nodes will continue to decrease the RMSEs, however, there are diminishing returns.

In practical scenarios, anchor nodes may not be equally spaced. Thus in Test 2, we use RSS measurements from randomly chosen anchor nodes. For example, we randomly choose four anchor nodes, and run AGAPE using the RSS measurements from these nodes. We repeat the above procedure 100 times, and each time calculate the RMSEs of

the position and orientation estimates. Similarly, we randomly choose seven, 10, 14, and 20 anchor nodes. The average RMSEs are shown as squares (■), and the RMSE standard deviations are shown as error bars in Fig. 9. From Fig. 9b, we see that the average orientation RMSEs in Test 2 are all larger than the RMSEs in Test 1. For position RMSEs shown in Fig. 9a, the average RMSEs in Test 2 are generally larger than the RMSEs in Test 1, except for the extreme case when the number of anchor nodes is four. Thus, the AGAPE algorithm generally performs better if the anchor nodes are equally spaced. However, the AGAPE algorithm is not very sensitive to the effect of anchor nodes being nonequally spaced. In fact, the differences between the position RMSEs in Test 1 and the average position RMSEs in Test 2 are always less than 0.4 m.

Finally, we compare the performance of the naive MLE 2D method with the AGAPE algorithm using randomly chosen nodes. As shown in Fig. 9a, the MLE 2D method is not very sensitive to the number of anchor nodes. However, the average position RMSEs from the MLE 2D method are always larger than those from the AGAPE algorithm for different numbers of anchor nodes.

### 3.6 Estimator Lower Bounds

One might think that the introduction of an additional unknown gain pattern model would increase the lower bound of the variance of an estimator. To see if that is true, we derive the Bayesian CRB [12] by including the gain pattern model parameters as nuisance parameters. We use the Bayesian CRB, because we have prior knowledge of the gain directionality $G_1$. We show that the CRB with an isotropic gain pattern assumption derived in [6] is a special case of the Bayesian CRB derived in this paper. Then, we compare the Bayesian CRB with and without isotropic gain pattern assumption. Our comparison shows that the introduction of a gain pattern model decreases the lower bound on the variance of a position estimator.

#### 3.6.1 Bayesian CRB

The gain pattern model expressed in (2) can be rewritten as

$$g(\alpha_i) = G_I \cos\alpha_i + G_Q \sin\alpha_i, \tag{15}$$

where $G_I = G_1 \cos\beta$, $G_Q = G_1 \sin\beta$.

To derive the Bayesian CRB, we assume that the orientation of the badge $\beta$ is uniformly distributed in the range of 0 to $2\pi$, because the orientation of the person wearing the badge is arbitrary. Next, we assume the in-phase component $G_I$ and quadrature component $G_Q$ of $G_1$ are i.i.d. Gaussian distributed with zero means and variance $\sigma_G^2$. $G_I$ and $G_Q$ are affected by many different aspects of the person's shape and size, and the badge placement, and thus may, by a central limit argument, be close to Gaussian. This assumption is equivalent to the assumption that $G_1$ is Rayleigh distributed [20], which agrees with our prior knowledge of $G_1$: 1) $G_1$ must be nonnegative and thus cannot be modeled as Gaussian or any distribution with infinite negative support; 2) $G_1$ may be small but is unlikely to be exactly zero for a person wearing a badge; and 3) $G_1$ is very unlikely to have very large values, since gain is related to (human) size. Improvement upon this distributional assumption must come from a population study with many participants, which we suggest for future research.

The Bayesian CRB is also called the Van Trees bound, or the MSE bound [12], it is given by

$$\mathrm{var}(\boldsymbol{\theta}) \geq (I_D + I_P)^{-1}, \tag{16}$$

where $\boldsymbol{\theta} = [\mathbf{z}_t^T, G_I, G_Q]^T$, $I_D$ is the Fisher information matrix, and $I_P$ is the prior information matrix [12]. Note that we only include the prior information of the gain pattern, no prior information of the badge position is included in the derivation of the Bayesian CRB.

All the elements in $I_D$ can be expressed as

$$[I_D]_{mn} = -E_P\left[E_D\left(\frac{\partial^2 \ln f_D}{\partial\boldsymbol{\theta}_m \partial\boldsymbol{\theta}_n}\right)\right], \tag{17}$$

where $E_D$ is the expectation with respect to data, $E_P$ is the expectation with respect to prior information of $\boldsymbol{\theta}$, and $f_D$ is the joint PDF of measurements $P_i$, which are assumed to be independent Gaussian with mean $\mu(\boldsymbol{\theta})$ and variance $\sigma^2$.

The elements of $I_P$ can be written as

$$[I_P]_{mn} = -E_P\left(\frac{\partial^2 \ln f_P}{\partial\boldsymbol{\theta}_m \partial\boldsymbol{\theta}_n}\right), \tag{18}$$

where $f_P$ is the PDF of the prior information of $\boldsymbol{\theta}$.

As shown in the supplemental material, which can be found on the Computer Society Digital Library at http://doi.ieeecomputersociety.org/10.1109/TMC.2011.89, the information matrix $I_D + I_P$ can be written as

$$I_D + I_P = I_{\boldsymbol{\theta}} = \begin{bmatrix} A_{11} & A_{12} \\ A_{21} & A_{22} \end{bmatrix}, \tag{19}$$

where

$$A_{11} = \begin{bmatrix} J_{xx} + M_{xy} & J_{xy} + N_{xy} \\ J_{xy} + N_{xy} & J_{yy} + M_{yx} \end{bmatrix}, \tag{20}$$

$$A_{12} = A_{21} = \begin{bmatrix} K_{xx} & K_{xy} \\ K_{xy} & K_{yy} \end{bmatrix}, \tag{21}$$

$$A_{22} = \begin{bmatrix} L_{xx} & L_{xy} \\ L_{xy} & L_{yy} \end{bmatrix}, \tag{22}$$

where $J_{xx} = J(\Delta x_{it}, \Delta x_{it})$, $K_{xx} = K(\Delta x_{it}, \Delta x_{it})$, $L_{xx} = L(\Delta x_{it}, \Delta x_{it})$, $M_{xx} = M(\Delta x_{it}, \Delta x_{it})$, $N_{xx} = N(\Delta x_{it}, \Delta x_{it})$, and $\Delta x_{it} = x_i - x_t$, and

$$J(u,v) = \frac{c^2}{\sigma^{2N}} \sum_{i=0}^{N-1} \frac{u}{d_{it}^2} \frac{v}{d_{it}^2}, \tag{23}$$

$$K(u,v) = \frac{c}{\sigma^{2N}} \sum_{i=0}^{N-1} \frac{uv}{d_{it}^3}, \tag{24}$$

$$L(u,v) = \frac{1}{\sigma^{2N}} \sum_{i=0}^{N-1} \frac{u}{d_{it}} \frac{v}{d_{it}} + \frac{1}{\sigma_G^2}, \tag{25}$$

$$M(u,v) = \frac{\sigma_G^2}{\sigma^{2N}} \sum_{i=0}^{N-1} \left(\frac{1}{d_{it}^2} + \frac{u^4}{d_{it}^6} + \frac{u^2 v^2}{d_{it}^6} - 2\frac{u^2}{d_{it}^4}\right), \tag{26}$$

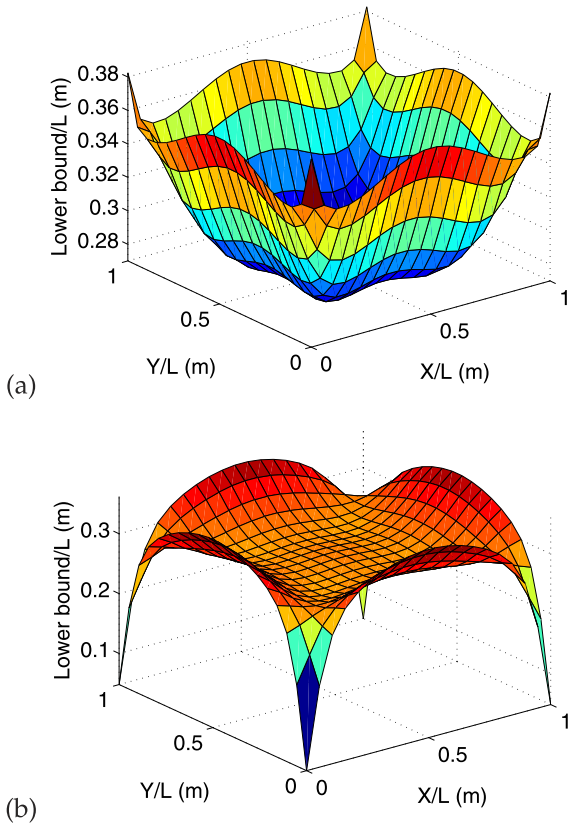


Fig. 10. Lower bounds. (a) Lower bound with $\sigma_G^2 = 0.0001$ (minimum value: 0.27, maximum value: 0.38); (b) Lower bound with $\sigma_G^2 = 1$ (minimum value: 0.05, maximum value: 0.36).

$$N(u,v) = \frac{\sigma_G^2}{\sigma^{2N}} \sum_{i=0}^{N-1} \left( \frac{u^3 v}{d_{it}^6} + \frac{v^3 u}{d_{it}^6} - 2\frac{uv}{d_{it}^4} \right), \tag{27}$$

where $c = \frac{10 n_p}{\ln 10}$.

### 3.6.2 Comparison with Related Literature

In related literature [6], a CRB is derived assuming the gain pattern is isotropic. In terms of the Bayesian CRB derived in this paper, the gain pattern term in the RSS-distance model is assumed to be zero. Since the RSS-distance model used in [6] can be considered as a special case of the RSS-distance model used here with $g(\alpha_i) = 0$, the Bayesian CRB derived here should be the same as the CRB derived in [6] when $\sigma_G^2$ approaches zero. This is shown next.

By using the blockwise matrix inversion, the inverse of the Fisher Information matrix can be written as

$$I_{\boldsymbol{\theta}}^{-1} = \begin{bmatrix} F_{11}^{-1} & -A_{11}^{-1} A_{12} F_{22}^{-1} \\ -F_{22}^{-1} A_{21} A_{11}^{-1} & F_{22}^{-1} \end{bmatrix}, \tag{28}$$

where $F_{11} = A_{11} - A_{12} A_{22}^{-1} A_{21}$ and $F_{22} = A_{22} - A_{21} A_{11}^{-1} A_{12}$.

In the limit as $\sigma_G^2 \to 0$, $M_{xy}$, $M_{yx}$, $N_{xy}$ all become zero, so we have

$$\lim_{\sigma_G^2 \to 0} A_{11} = \begin{bmatrix} J_{xx} & J_{xy} \\ J_{xy} & J_{yy} \end{bmatrix} \triangleq J, \tag{29}$$

$$\lim_{\sigma_G^2 \to 0} A_{22} = \begin{bmatrix} L_{xx} & L_{xy} \\ L_{xy} & L_{yy} \end{bmatrix} = \infty. \tag{30}$$

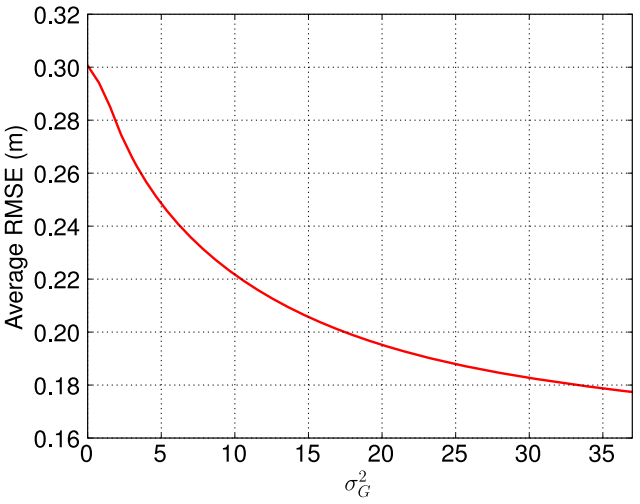


Fig. 11. RMSE bounds as a function of $\sigma_G^2$.

Thus, $F_{11} = A_{11}$, and $F_{22}^{-1} = 0$. So the inverse of the Fisher information matrix becomes

$$\lim_{\sigma_G^2 \to 0} I_{\boldsymbol{\theta}}^{-1} = \begin{bmatrix} J^{-1} & 0 \\ 0 & 0 \end{bmatrix}. \tag{31}$$

Notice that (29) is the same as [6, (10)], which assumes isotropic gain pattern. This proves that the CRB derived in [6] is a special case of the Bayesian CRB derived here, and if $\sigma_G^2$ approaches zero, the Bayesian CRB converges to the CRB derived previously.

### 3.6.3 Discussion

From (23) to (27), we see that the Bayesian CRB not only depends on radio channel parameters $n_p$ and $\sigma^2$, but also depends on gain pattern parameter $\sigma_G^2$. Once we have these three parameters, we can calculate the Bayesian CRB for an L m by L m square area surrounded by four anchor nodes located at each corner.

Using the same channel parameters as [6] ($n_p/\sigma = 1.7$), the Bayesian CRBs with two different $\sigma_G^2$ are shown in Fig. 10. As expected, if $\sigma_G^2$ is very close to zero, e.g., $\sigma_G^2 = 0.0001$, the Bayesian CRB is identical to the CRB derived in [6], as shown in Fig. 10a. If $\sigma_G^2$ is not close to zero, e.g., $\sigma_G^2 = 1$, the Bayesian CRB is shown in Fig. 10b. From the comparison of Figs. 10a and 10b, we see that the maximum value and minimum value of Bayesian CRB are both lower than the CRB with an isotropic gain pattern assumption. If we introduce the "average RMSE bound" as the average value of the square root of the Bayesian CRB bounds over this L m by L m area, the average RMSE bound for $\sigma_G^2 = 1$ is 0.29 m, which is also lower than the 0.30 m average RMSE bound with $\sigma_G^2 = 0.0001$.

Further, the average RMSE bounds with different $\sigma_G^2$ are shown in Fig. 11. Since higher $\sigma_G^2$ represents higher directionality $G_1$, we see that the RMSE bound is lower if the directionality of the gain pattern is higher. Note that we assume the number of anchor nodes that can receive the signal transmitted from the badge stays fixed for all $\sigma_G^2$.

In sum, we conclude that the RMSE bound with a directional gain pattern assumption could be lower than the RMSE bound with an isotropic gain pattern assumption. For the directional gain pattern case, we would benefit

more, i.e., have a lower RMSE bound from a gain pattern with a higher directionality, if the number of nodes that can hear the badge stays fixed.

## 4 Tracking

In this section, we introduce an improved tracking method that takes advantage of the user's orientation estimate from the AGAPE algorithm, and that people generally walk in the direction they are facing. We develop a novel Kalman filter which additionally tracks user orientation, and uses this to further improve coordinate tracking. Traditional Kalman filters and extended Kalman filters use only coordinate estimates as input, even though they are used to estimate velocity (and thus direction). Our orientation enhanced extended Kalman filter is distinct because it uses estimated orientation *as an input*, in addition to providing estimated velocity. We also compare the tracking results from traditional Kalman filters and our OE-EKF. The results show that without any additional measurements, the OE-EKF is noticeably more robust to large errors.

### 4.1 Kalman Filter

In the traditional Kalman filter, the current state vector, which in this case includes both mobile's position and velocity, is related to the previous state by the following model:

$$\mathbf{s}[n] = A\mathbf{s}[n-1] + \mathbf{u}[n], \tag{32}$$

where the state vector $\mathbf{s} = [P_x, P_y, V_x, V_y]^T$, the driving noise $\mathbf{u} = [0, 0, u_x, u_y]^T$, and matrix $A$ is

$$A = \begin{bmatrix} 1 & 0 & 1 & 0 \\ 0 & 1 & 0 & 1 \\ 0 & 0 & 1 & 0 \\ 0 & 0 & 0 & 1 \end{bmatrix}. \tag{33}$$

For the traditional Kalman filter without orientation in the measurement vector, the observation model is

$$\mathbf{x}[n] = H\mathbf{s}[n] + \mathbf{w}[n], \tag{34}$$

where the measurement vector $\mathbf{x} = [\hat{x}_t, \hat{y}_t]^T$ is from the coordinate estimates from the AGAPE algorithm. The measurement noise $\mathbf{w} = [w_x, w_y]^T$, and the observation matrix $H$ is

$$H = \begin{bmatrix} 1 & 0 & 0 & 0 \\ 0 & 1 & 0 & 0 \end{bmatrix}. \tag{35}$$

### 4.2 Orientation-Enhanced Extended Kalman Filter

As discussed in Section 3.4, the AGAPE algorithm can produce both position and orientation estimates of a mobile person. Here, we propose a novel Kalman filter that uses the output of the AGAPE algorithm as input to the tracking algorithm. If we include the mobile person's orientation in the Kalman filter, the state model (32) remains the same. However, the observation model becomes nonlinear, because the orientation cannot be explicitly expressed as a linear function of the state vector. Thus, the extended Kalman filter must be used. Since we add orientation information in the measurement vector, we call it orientation-enhanced extended Kalman filter.

The observation model of the OE-EKF is

$$\mathbf{x}[n] = \mathbf{h}(\mathbf{s}[n]) + \mathbf{w}[n], \tag{36}$$

where $\mathbf{h}$ is the nonlinear function relating state vector $\mathbf{s}$ to measurement vector $\mathbf{x}$.

If the mobile person is moving forward, then the orientation $\beta$ of that person can be expressed as the arctangent of the ratio of Y component of velocity to X component of velocity. If the mobile person is moving backward, then there is a 180 degrees difference between $\beta$ and the arctangent function. Because in most situations people move forward, his or her orientation can be expressed as

$$\beta = \operatorname{atan}\left(\frac{V_y}{V_x}\right), \tag{37}$$

where $V_y$ and $V_x$ are the Y component and X component of velocity, respectively.

To avoid the ambiguity of $\pi$ or $-\pi$ from arctangent function, instead of directly using $\beta$, we use $\cos\beta$ and $\sin\beta$ in the measurement vector. So for the extended Kalman filter, the measurement vector becomes

$$\mathbf{x} = \left[P_x, P_y, \cos\beta, \sin\beta\right]^T. \tag{38}$$

Accordingly, $\mathbf{h}(\mathbf{s})$ in the new measurement model equation becomes

$$\mathbf{h}(\mathbf{s}) = \left[P_x, P_y, \frac{V_x}{\sqrt{V_x^2 + V_y^2}}, \frac{V_y}{\sqrt{V_x^2 + V_y^2}}\right]^T. \tag{39}$$

Then, the Jacobian matrix can be written as

$$J = \frac{\partial \mathbf{h}(\mathbf{s})}{\partial \mathbf{s}} = \begin{bmatrix} 1 & 0 & 0 & 0 \\ 0 & 1 & 0 & 0 \\ 0 & 0 & J_{33} & J_{34} \\ 0 & 0 & J_{43} & J_{44} \end{bmatrix}, \tag{40}$$

where

$$\begin{aligned} J_{33} &= \frac{\partial}{\partial V_x}\left(V_x/\sqrt{V_x^2 + V_y^2}\right), \\ J_{34} &= \frac{\partial}{\partial V_y}\left(V_x/\sqrt{V_x^2 + V_y^2}\right), \\ J_{43} &= \frac{\partial}{\partial V_x}\left(V_y/\sqrt{V_x^2 + V_y^2}\right), \\ J_{44} &= \frac{\partial}{\partial V_y}\left(V_y/\sqrt{V_x^2 + V_y^2}\right). \end{aligned}$$

Once we have the Jacobian matrix, the OE-EKF is implemented following the basic equations in [21].

### 4.3 Experimental Results

Using the same data collected from the outdoor experiments discussed in Section 3.5.2, and using the output of the AGAPE algorithm, we apply the Kalman filter and OE-EKF to track the person wearing the badge.

For Experiment 1, the position tracking results from the Kalman filter and OE-EKF are shown in Fig. 12. We see that due to the lack of previous measurements, the first position tracking result is more than 1 meter away from the actual

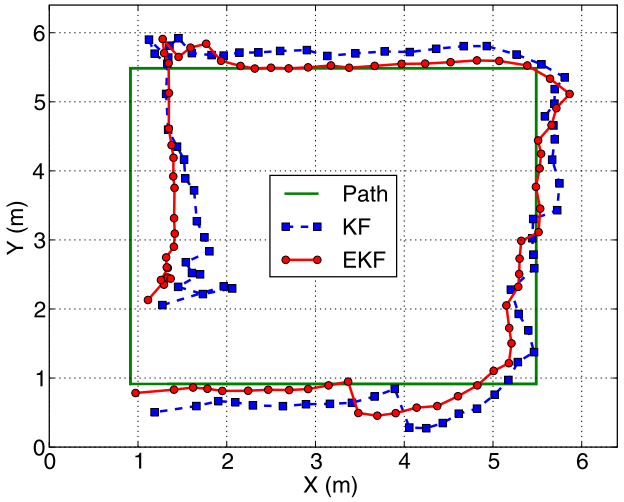


Fig. 12. Position estimates from KF (■) and from OE-EKF (•) (only the first round tracking results from Experiment 1 are shown here).

position for both the Kalman filter and the OE-EKF. However, as more and more measurements are available, the tracking errors become generally less than 0.5 meters.

From the comparison of the Kalman filter and OE-EKF tracking results, we see that with the help of orientation estimates from the AGAPE algorithm, the position tracking from the OE-EKF is more accurate than that from the Kalman filter. We note that if the variance of orientation estimate is set to be a very large number, then the tracking result from the OE-EKF is almost identical to that of the Kalman filter. That is, if little weight is given to the observation of the orientation, our OE-EKF is simplified to the Kalman filter.

The orientation tracking results from the OE-EKF are shown in Fig. 13. Compared to the orientation estimates from the AGAPE algorithm, the estimated orientations from the OE-EKF are closer to the actual orientation when the user is walking along a straight line. However, at each corner of the square path, when the user changes direction suddenly by 90 degrees, the OE-EKF needs several measurements to adjust orientation estimates to the correct directions. This overshoot problem at points of high acceleration is very common for a Kalman filter tracking

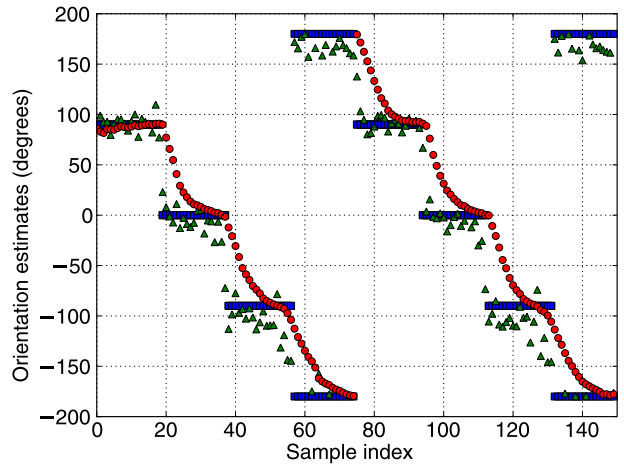


Fig. 13. Orientation estimates from OE-EKF (•) and from AGAPE (△).

TABLE 2
Experimental Tracking Results: RMSEs from KF without Gain, KF with Gain and OE-EKF

| RMSE (in meter) | KF without gain | KF with gain | OE-EKF |
|---|---|---|---|
| Experiment 1 | 2.25 | 0.50 | 0.44 |
| Experiment 2 | 2.63 | 0.57 | 0.56 |
| Experiment 3 | 2.37 | 0.52 | 0.46 |

method, and can be minimized with more complicated models of movement dynamics and measurement noise [22], however, these are not in the scope of this paper.

To quantify the improvement that the gain pattern and the orientation estimate from the AGAPE algorithm can make in tracking, the RMSEs from the following three tracking methods are listed in Table 2.

- KF without gain: the Kalman filter using position estimate from the naive MLE method with an isotropic gain pattern assumption.
- KF with gain: the Kalman filter using position estimate from AGAPE.
- OE-EKF: the extended Kalman filter using both position and orientation estimates from AGAPE.

From Table 2, we see that the RMSEs from KF without gain method are all above 2.0 m for three experiments. For KF with gain method, which only uses position estimates from AGAPE as input, the average RMSE of the three experiments is 0.53 m. Since both the position estimate and orientation estimate from the AGAPE algorithm are used in OE-EKF, the RMSEs from OE-EKF method are further reduced compared to KF with gain method for all three experiments.

The CDFs of the position tracking errors from these three tracking methods are shown in Fig. 14. The median error for KF without gain method is about 2.3 m, while the median errors for KF with gain and OE-EKF methods are both about 0.4 m. However, OE-EKF method has 95 percent of tracking errors less than 0.76 m, while KF with gain method has 95 percent of tracking errors less than 0.90 m. In this case, OE-EKF shows 16.7 percent improvement. Using the 95 percentile of errors shows the robustness to large errors.

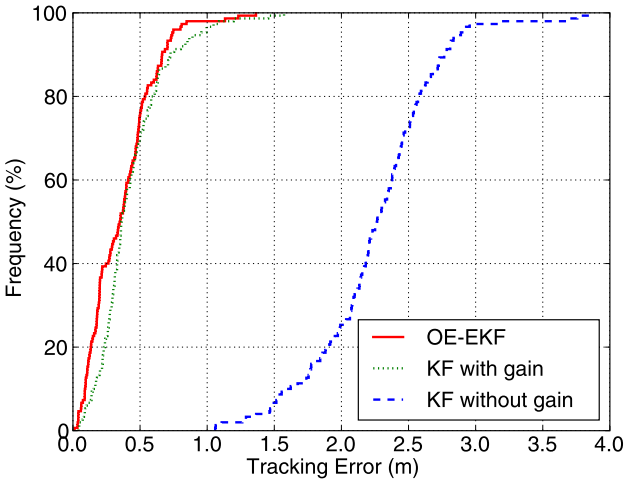


Fig. 14. CDFs comparison of different tracking methods using data from Experiment 1.

The experimental results show that OE-EKF is more robust to large errors without any additional measurements.

In OE-EKF, we assume that people walk forward with the badge on their front. If badges were consistently worn on a different side, that side could be estimated and the tracking algorithm adjusted accordingly. If this assumption was often violated (e.g., if the person walked backward or sideways), KF with gain method would likely perform better than OE-EKF.

## 5 Related Work

In wireless sensor network localization, many kinds of measurements can be used: angle of arrival (AOA), time of arrival (TOA), time difference of arrival (TDOA), received signal strength, etc. [23]. This work uses estimated angle (orientation) of the badge in the position estimation, however, it is not like the AOA-based localization. In AOA-based localization, anchor nodes measure the angle from which power arrives at a receiver using a directional antenna. We do not use any directional antenna—anchor nodes only measure RSS. Moreover, we estimate a user's facing direction (orientation), not the direction to any other device. For RSS-based localization, many algorithms have been proposed to improve the localization accuracy [24], [7], [25]. The performance of RSS-based localization algorithms are limited by the irregularities in measured RSS. Variation in RSS is caused by the presence of multipath, shadowing caused by the presence of obstacles in the environment, and also nonuniformity of the antenna gain pattern [26], [27]. Little effort has been made toward including gain pattern in model-based RSS localization algorithms.

Many localization studies have already shown the effect of human body orientation on RSS measurements [1], [8], [9], [10]. Kaemarungsi and Krishnamurthy [10] examine the effects of the human body orientation on RSS measurements using four different user's orientations (facing North, West, South, and East). Their experiments show that the mean RSS of one orientation, at which the user body blocks the LOS could be more than 9.0 dB lower than that of another orientation. Experiments performed by King et al. [5] measure the RSS every 45 degrees while a person carrying a mobile device turns around. Their experimental results show that the RSS increases nearly 15 dB in case of a direct LOS between a receiver and an access point. In this paper, we also perform a measurement campaign to study the variation of RSS as a function of user orientation. The results of our measurement campaign agree with the findings of King et al. [5], and we further provide a model that quantifies RSS measurements as a function of user orientations.

Other research has independently determined that user orientation is significant in improving the localization accuracy [28], [29]. However, these methods determine the effect of the user orientation based on a separate training campaign, which consumes significant human effort and time. This paper provides a statistical model to quantify the effect of human body orientation on RSS, which could simplify the fingerprint database construction. Thus, our work can improve model-based localization, and is also complementary to fingerprint-based localization.

## 6 Conclusion

In this paper, we model the variation of RSS due to the human body as a cosine function of the orientations of the body, and we propose a first-order sinusoidal model that is useful for user orientation estimation from multiple RSS measurements. We implement the AGAPE algorithm to estimate both the position and the orientation of the user. We also implement an OE-EKF by including orientation estimate in tracking. Experimental results show that estimating the nonisotropic gain pattern can greatly improve both localization and tracking of people in RF sensor networks.

## Acknowledgments

The authors would like to acknowledge the contributions of Jessica Croft, Dustin Maas, and Joey Wilson, who assisted in the experiments. This material is based upon work supported by the US National Science Foundation under Grant Nos. #0748206 and #1035565. M. Rabbat was supported by the Natural Sciences and Engineering Research Council of Canada (NSERC) and the *Fonds québécois de la recherche sur la nature et les technologies (FQRNT)*.

## References

[1] P. Bahl and V.N. Padmanabhan, "RADAR: An In-Building RF-Based User Location and Tracking System," *Proc. IEEE INFOCOM,* vol. 2, pp. 775-784, 2000.

[2] N. Patwari, J. Ash, S. Kyperountas, R.M. Moses, A.O. Hero III, and N.S. Correal, "Locating the Nodes: Cooperative Localization in Wireless Sensor Networks," *IEEE Signal Processing Magazine,* vol. 22, no. 4, pp. 54-69, July 2005.

[3] M. Jensen and Y. Rahmat-Samii, "EM Interaction of Handset Antennas and a Human in Personal Communications," *Proc. IEEE,* vol. 83, no. 1, pp. 7-17, Jan. 1995.

[4] J. Griffin and G. Durgin, "Complete Link Budgets for Backscatter Radio and RFID Systems," *IEEE Antennas and Propagation Magazine,* vol. 51, no. 2, pp. 11-25, Apr. 2009.

[5] T. King, S. Kopf, T. Haenselmann, C. Lubberger, and W. Effelsberg, "COMPASS: A Probabilistic Indoor Positioning System Based on 802.11 and Digital Compasses," *Proc. ACM First Int'l Workshop Wireless Network Testbeds, Experimental Evaluation & Characterization (WiNTECH '06),* Sept. 2007.

[6] N. Patwari, A.O. Hero III, M. Perkins, N. Correal, and R.J. O'Dea, "Relative Location Estimation in Wireless Sensor Networks," *IEEE Trans. Signal Processing,* vol. 51, no. 8, pp. 2137-2148, Aug. 2003.

[7] T. Roos, P. Myllymki, H. Tirri, P. Misikangas, and J. Sievnen, "A Probabilistic Approach to WLAN User Location Estimation," *Int'l J. Wireless Information Networks,* vol. 9, no. 3, pp. 155-164, 2002.

[8] A. Ladd, K. Bekris, G. Marceau, A. Rudys, L. Kavraki, and D. Wallach, "Robotics-Based Location Sensing Using Wireless Ethernet," *Proc. ACM MobiCom,* pp. 227-238, Sept. 2002.

[9] A. Howard, S. Siddiqi, and G. Sukhatme, "An Experimental Study of Localization Using Wireless Ethernet," *Proc. Int'l Conf. Field and Service Robotics,* pp. 201-206, 2003.

[10] K. Kaemarungsi and P. Krishnamurthy, "Properties of Indoor Received Signal Strength for WLAN Location Fingerprinting," *Proc. First Ann. Int'l Conf. Mobile and Ubiquitous Systems: Networking and Services (MobiQuitous '04),* pp. 14-23, 2004.

[11] A. Awad, T. Frunzke, and F. Dressler, "Adaptive Distance estimation and Localization in wsn Using rssi Measures," *Proc. 10th EUROMICRO Conf. Digital System Design - Architectures, Methods and Tools (DSD '07),* pp. 471-478, Aug. 2007.

[12] H.L. Van Trees, *Detection, Estimation, and Modulation Theory,* Part I. John Wiley & Sons, 1968.

[13] T.S. Rappaport, *Wireless Communications: Principles and Practice.* Prentice-Hall, Inc., 1996.

[14] W.L. Stutzman and G.A. Theile, *Antenna Theory and Design.* John Wiley & Sons, 1981.
[15] A.V. Oppenheim and R.W. Schafer, *Discrete-Time Signal Processing.* Prentice Hall, 2009.
[16] Chipcon Products from Texas Instruments, *CC2431: System-on-Chip for 2.4 GHz ZigBee/IEEE 802.15.4 with Location Engine,* Sept. 2005.
[17] N. Lomb, "Least-Squares Frequency Analysis of Unequally Spaced Data," *Astrophysics and Space Science,* vol. 39, pp. 447-462, 1976.
[18] A. Gunawardana and W. Byrne, "Convergence Theorems for Generalized Alternating Minimization Procedures," *J. Machine Learning Research,* vol. 6, pp. 2049-2073, 2005.
[19] "Sensing and Processing Across Networks at Utah," http://span.ece.utah.edu/spin, 2011.
[20] S. Miller and D. Childers, *Probability and Random Processes: With Applications to Signal Processing and Communications.* Academic, 2004.
[21] S.M. Kay, *Fundamentals of Statistical Signal Processing.* Prentice Hall, 1993.
[22] M. Friedmann, T. Stamer, and A. Pentland, "Device Synchronization Using an Optimal Linear Filter," *Proc. Symp. Interactive 3D Graphics,* pp. 57-62, 1992.
[23] G. Mao, B. Fidan, and B.D.O. Anderson, "Wireless Sensor Network Localization Techniques," *Computer Networks,* vol. 51, no. 10, pp. 2529-2553, 2007.
[24] A. Savvides, C. Han, and M. Strivastava, "Dynamic Fine-Grained Localization in Ad-Hoc Networks of Sensors," *Proc. Seventh Ann. Int'l Conf. Mobile Computing and Networking,* pp. 166-179, 2001.
[25] K. Yedavalli, B. Krishnamachari, S. Ravula, and B. Srinivasan, "Ecolocation: A Sequence Based Technique for RF-Only Localization in Wireless Sensor Networks," *Proc. Fourth Int'l Conf. Information Processing in Sensor Networks (IPSN '05),* Apr. 2005.
[26] D. Kotz, C. Newport, and C. Elliott, "The Mistaken Axioms of Wireless-Network Research," Technical Report TR2003-467, Dept. of Computer Science, Dartmouth College, http://www.cs.dartmouth.edu/reports/abstracts/TR2002-467, July 2003.
[27] G. Zhou, T. He, S. Krishnamurthy, and J. Stankovic, "Impact of Radio Irregularity on Wireless Sensor Networks," *Proc. ACM MobiSys,* pp. 125-138, 2004.
[28] C. Röhrig and F. Künemund, "Estimation of Position and Orientation of Mobile Systems in a Wireless LAN," *Proc. 46th IEEE Conf. Decision and Control,* pp. 4932-4937, Dec. 2007.
[29] I.-E. Liao and K.-F. Kao, "Enhancing the Accuracy of WLAN-Based Location Determination Systems Using Predicted Orientation Information," *Information Sciences,* vol. 178, pp. 1049-1068, 2008.

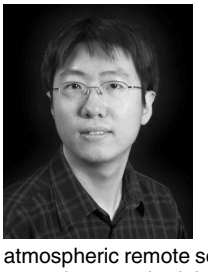

**Yang Zhao** received the BS degree in electrical engineering from Shandong University in 2003 and the MS degree in electrical engineering from the Beijing University of Aeronautics and Astronautics in 2006. He is currently working toward the PhD degree in electrical and computer engineering at the University of Utah. He studied radar signal processing at the Beijing University of Aeronautics and Astronautics between 2003 and 2006, and developed retrieval algorithms for atmospheric remote sensing at the University of Utah between 2006 and 2009. In 2009, he joined the Sensing and Processing Across Networks (SPAN) lab and started research on location estimation in wireless sensor networks. His current research includes RFID badge localization and radio device-free localization. He is a student member of the IEEE.

**Neal Patwari** received the BS (1997) and MS (1999) degrees from Virginia Tech and the PhD degree from the University of Michigan, Ann Arbor (2005), all in electrical engineering. He was a research engineer at Motorola Labs, Florida, between 1999 and 2001. Since 2006, he has been at the University of Utah, where he is an assistant professor in the Department of Electrical and Computer Engineering, with an adjunct appointment in the School of Computing. He directs the Sensing and Processing Across Networks (SPAN) Lab, which performs research at the intersection of statistical signal processing and wireless networking. His research interests are in radio channel signal processing, in which radio channel measurements are used to improve security and networking and to perform localization. He received the US National Science Foundation CAREER Award in 2008, the 2009 IEEE Signal Processing Society Best Magazine Paper Award, and the 2011 University of Utah Early Career Teaching Award. He has served on technical program committees for IEEE conferences SECON, ICDCS, DCOSS, ICC, RTAS, WoWMoM, ICCCN, and MILCOM. He is an associate editor of the *IEEE Transactions on Mobile Computing*. He is a member of the IEEE.

**Piyush Agrawal** has been working toward the PhD degree in electrical engineering at the University of Utah in Salt Lake City since 2008, where he also received the MEEE in Fall 2008. His research interests lies in developing better statistical models for received signal strength in ad hoc and sensor networks. His current research is focused on improving the RSS-based localization algorithms for infrastructure-wide wireless network deployments. He is a student member of the IEEE.

**Michael G. Rabbat** received the BSc degree from the University of Illinois at Urbana-Champaign (2001), the MSc degree from Rice University (2003), and the PhD degree from the University of Wisconsin-Madison (2006), all in electrical engineering. He is currently an assistant professor at McGill University. He was a visiting researcher at Applied Signal Technology, Inc., during the summer of 2003. He received the Best Paper Award (Signal Processing and Information Theory Track) at the 2010 IEEE Conference on Distributed Computing in Sensor Systems, Outstanding Student Paper Honorable Mention at the 2006 Conference on Neural Information Processing Systems, the Best Student Paper Award at the 2004 ACM/IEEE Conference on Information Processing in Sensor Networks, and the Harold A. Peterson Thesis Prize. His research interests include distributed signal processing, information processing in sensor networks, network monitoring, and network inference. He is currently an associate editor for the *ACM Transactions on Sensor Networks*. He is a member of the IEEE.